Dynamic NMR Study of the Tautomerism of Bicyclic Oxalamidines: Kinetic HH/HD/DD Isotope and Solvent Effects

Gerd Scherer and Hans-Heinrich Limbach*

Contribution from the Institut für Organische Chemie der Freien Universität Berlin, Takustrasse 3, D-14195 Berlin, Federal Republic of Germany

Received April 26, 1993. Revised Manuscript Received October 19, 1993[⊗]

Abstract: The tautomerism of oxalamidine, which consists of an intramolecular degenerate double proton transfer between nitrogen atoms, has been studied by dynamic NMR spectroscopy. Experiments were performed on two bicyclic oxalamidines, 2,2'-bis(3,4,5,6-tetrahydro-1,3-diazine) (OA6) and 2,2'-bis(4,5,6,7-tetrahydro-1,3-diazepine) (OA7) dissolved in organic solvents. For this purpose, both compounds had to be labeled with ^{15}N and partly with ^2H. The tautomerism of OA6 was too slow to be detectable by NMR, in contrast to the case of OA7. Rate constants of the tautomerism of OA7 dissolved in methylcyclohexane-d_{14} (MCY) and in acetonitrile d_3 (AN) could be obtained, including the full kinetic HH/HD/DD isotope effects. The data for MCY can be represented by the following: $k_{MCY}^{HH} = 10^{11.2\pm0.1}$ exp(-57.6 ± 06 kJ mol^{-1}/RT) s^{-1}, 303 K $\leq T \leq$ 415 K, $k_{298 K}^{HH} = 14$ s^{-1}; $k_{MCY}^{HD} = 10^{11.1\pm0.1}$ exp(-59.6 ± 1.0 kJ mol^{-1}/RT) s^{-1}, 340 K $\leq T \leq$ 415 K, $k_{298 K}^{HD} = 4.4$ s^{-1}; $k_{MCY}^{DD} = 10^{10.9\pm0.1}$ exp(-59.5 ± 0.7 kJ mol^{-1}/RT) s^{-1}, 303 K $\leq T \leq$ 415 K, $k_{298 K}^{DD} = 2.9$ s^{-1}. From these data, we determine that $k_{MCY}^{HH}/k_{MCY}^{HD} \approx 3.1$, $k_{MCY}^{HH}/k_{MCY}^{DD} \approx 4.8$, and $k_{MCY}^{HD}/k_{MCY}^{DD} \approx 1.5$ at 298 K. The data for AN are as follows: $k_{AN}^{HH} = 10^{11.7\pm0.1}$ exp(-56.2 ± 0.9 kJ mol^{-1}/RT) s^{-1}, 300 K $\leq T \leq$ 382 K, $k_{298 K}^{HH} = 75$ s^{-1}; $k_{AN}^{HD} = 10^{11.5\pm0.1}$ exp(-57.6 ± 1.4 kJ mol^{-1}/RT) s^{-1}, 312 K $\leq T \leq$ 374 K, $k_{298 K}^{HD} = 23$ s^{-1}; and $k_{AN}^{DD} = 10^{11.1\pm0.2}$ exp(-56.7 ± 1.2 kJ mol^{-1}/RT) s^{-1}, 300 K $\leq T \leq$ 393 K, $k_{298 K}^{DD} = 15$ s^{-1}. From these data, we determine that $k_{AN}^{HH}/k_{AN}^{HD} = 3.2$, $k_{AN}^{HH}/k_{AN}^{DD} = 5.2$, $k_{AN}^{HD}/k_{AN}^{DD} = 1.6$, and $k_{AN}^{HH}/k_{MCY}^{HH} = 5.4$ at 298 K. No dependence of chemical shifts nor of rate constants on concentration was observed, which indicates that OA7 is not subject to intermolecular hydrogen bonding. Therefore, the observed increase of the rate constants with solvent polarity indicates the formation of a highly polar transition state, as expected for a stepwise proton transfer. This interpretation is independently supported by the observed multiple kinetic solvent isotope effects. The size of the kinetic isotope effects indicates a substantial heavy atom reorganization preceding each single proton-transfer step. The differing dynamic behavior of OA6 and OA7 indicates that this phenomenon consists not only of solvent reorganization but mainly of a compression of the hydrogen bond in which the proton transfer takes place. In the bicyclic oxalamidines, this compression is more or less coupled to an elongation of the other hydrogen bond and/or to a reorganization of the methylene bridges.

Multiple proton transfers play an important role in a number of organic and biochemical reactions.[1–5] Information on the reaction mechanisms can be obtained by measuring multiple kinetic hydrogen/deuterium isotope effects. To understand the factors which influence the latter, degenerate, well-defined intramolecular and intermolecular multiple proton-transfer reaction systems have, in particular, been studied during recent years in our laboratory.[5–20] Rate constants were derived by NMR line-shape analyses and magnetization-transfer experiments. In

the case of the degenerate intramolecular double proton and deuteron transfers in porphyrins and in azophenine (Figure 1), it was found that replacement of the first H by D led to a substantial reduction of the reaction rates, whereas replacement of the second H by D gave rise to only a small decrease. Initially, we thought that this result was compatible with proton tunneling along a concerted reaction pathway (Figure 1a).[6a] However, as more examples were studied, it became clear that two large HH/HD and HD/DD isotope effects should be expected for the concerted

* Abstract published in *Advance ACS Abstracts*, January 15, 1994.

(1) Gandour, R. D.; Schowen, R. L. *Transition States of Biochemical Processes*; Plenum Press: New York, 1978.

(2) Cook, P. F. *Enzyme Mechanisms from Isotope Effects*; Wiley: New York, 1992.

(3) Schuster, P.; Zundel, G.; Sandorfy, C., Eds. *The Hydrogen Bond*; North Holland Publ. Co.: Amsterdam, 1976.

(4) Limbach, H.-H. In *Aggregation Process in Solution*; Wyn-Jones, E., Gormally, J., Eds.; Elsevier: Amsterdam, 1983; Chapter 16, p 410.

(5) Limbach, H. H. *Dynamic NMR Spectroscopy in the Presence of Kinetic Hydrogen/Deuterium Isotope Effects. NMR—Basic Principles and Progress*; Springer: Heidelberg, 1991; Vol. 23, Chapter 2.

(6) (a) Limbach, H. H.; Hennig, J.; Gerritzen, D.; Rumpel, H. *Faraday Discuss. Chem. Soc.* 1982, 74, 229. (b) Schlabach, M.; Wehrle, B.; Rumpel, H.; Braun, J.; Scherer, G.; Limbach, H. H. *Ber. Bunsenges. Phys. Chem.* 1992, 96, 821.

(7) Hennig, J.; Limbach, H. H. *J. Magn. Reson.* 1982, 49, 322.

(8) Hennig, J.; Limbach, H. H. *J. Am. Chem. Soc.* 1984, 106, 292.

(9) Gerritzen, D.; Limbach, H.-H. *J. Am. Chem. Soc.* 1984, 106, 869.

(10) Meschede, L.; Gerritzen, D.; Limbach, H. H. *Ber. Bunsenges. Phys. Chem.* 1988, 92, 469. Limbach, H. H.; Meschede, L.; Scherer, G. *Z. Naturforsch.* 1989, 44a, 459. Meschede, L.; Limbach, H. H. *J. Phys. Chem.* 1991, 95, 10267.

(11) Rumpel, H.; Limbach, H.-H. *J. Am. Chem. Soc.* 1989, 111, 5429. Rumpel, H.; Limbach, H.-H.; Zachmann, G. *J. Phys. Chem.* 1989, 93, 1812.

(12) Otting, G.; Rumpel, H.; Meschede, L.; Scherer, G.; Limbach, H.-H. *Ber. Bunsenges. Phys. Chem.* 1986, 90, 1122.

(13) Scherer, G.; Limbach, H. H. *J. Am. Chem. Soc.* 1989, 111, 5946.

(14) Schlabach, M.; Rumpel, H.; Limbach, H. H. *Angew. Chem.* 1989, 101, 84; *Angew. Chem., Int. Ed. Engl.* 1989, 28, 76. Schlabach, M.; Scherer, G.; Limbach, H. H. *J. Am. Chem. Soc.* 1991, 113, 3550. Schlabach, M.; Limbach, H. H.; Shu, A.; Bunnenberg, E.; Tolf, B.; Djerassi, C. *J. Am. Chem. Soc.* 1993, 115, 4554.

(15) Limbach, H. H.; Hennig, J.; Kendrick, R. D.; Yannoni, C. S. *J. Am. Chem. Soc.* 1984, 106, 4059. Wehrle, B.; Limbach, H. H.; Köcher, M.; Ermer, O., Vogel, E. *Angew. Chem.* 1987, 99, 914; *Angew. Chem., Int. Ed. Engl.* 1987, 26, 934. Limbach, H. H.; Wehrle, B.; Schlabach, M.; Kendrick, R. D.; Yannoni, C. S. *J. Magn. Reson.* 1988, 77, 84.

(16) Limbach, H. H.; Wehrle, B.; Zimmermann, H.; Kendrick, R. D.; Yannoni, C. S. *J. Am. Chem. Soc.* 1987, 109, 929. Limbach, H. H.; Wehrle, B.; Zimmermann, H.; Kendrick, R. D.; Yannoni, C. S. *Angew. Chem.* 1987, 99, 241; *Angew. Chem., Int. Ed. Engl.* 1987, 26, 247. Wehrle, B.; Limbach, H. H.; Zimmermann, H. *J. Am. Chem. Soc.* 1988, 110, 7014.

(17) Wehrle, B.; Limbach, H. H. *Chem. Phys.* 1989, 136, 223.

(18) Aguilar-Parrilla, F.; Wehrle, B.; Bräunling, H.; Limbach, H. H. *J. Magn. Reson.* 1990, 87, 592.

(19) Butenhoff, T.; Moore, C. B. *J. Am. Chem. Soc.* 1988, 110, 8336.

(20) Butenhoff, T.; Chuck, R.; Limbach, H. H.; Moore, C. B. *J. Phys. Chem.* 1990, 94, 7847.
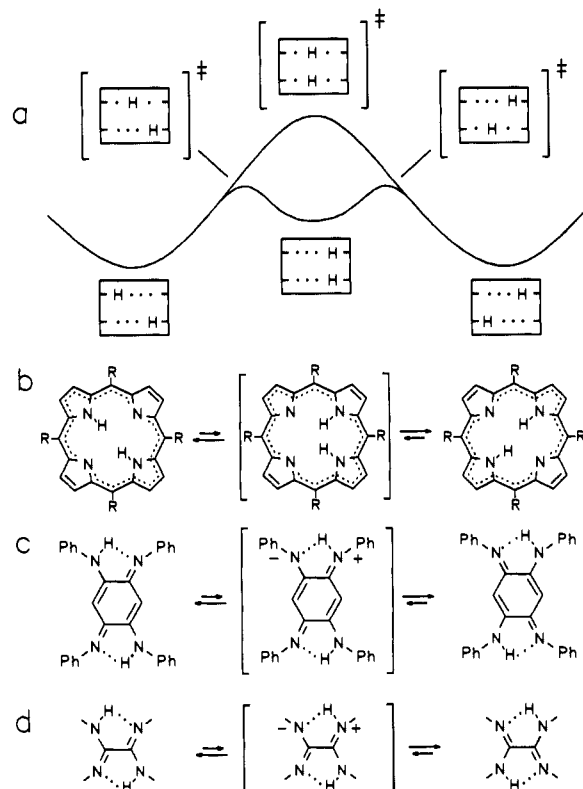
Figure 1. Pathways of a degenerate intramolecular double proton transfer. (a) Free energy reaction profiles (schematically) for the concerted and the stepwise reaction pathways. The tautomerism of (b) porphyrins,[6,7,8,14] (c) azophenine (AP),[11] and (d) oxalamidine.
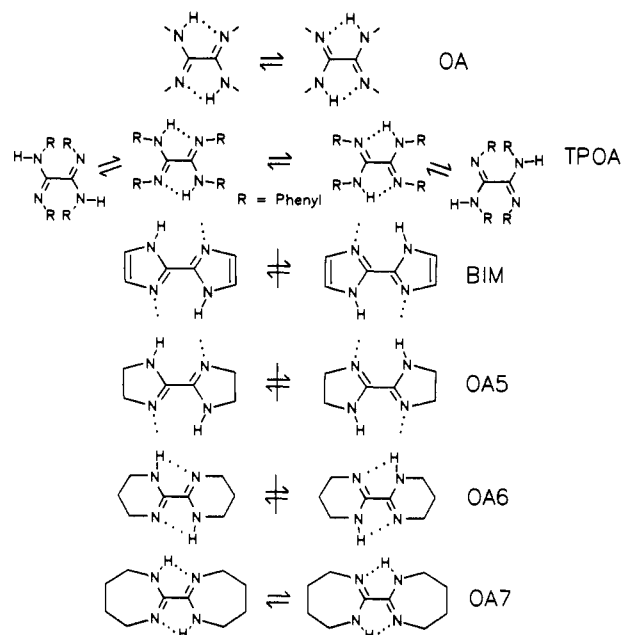

Figure 2. Intramolecular tautomerism of oxalamidines. OA, parent compound; TPOA, tetraphenyloxalamidine;[12] BIM, bisimidazolyl; OA5, 2,2′-bis(4,5-dihydro-1,3-diazole); OA6, 2,2′-bis(3,4,5,6-tetrahydro-1,3-diazine); OA7, 2,2′-bis(4,5,6,7-tetrahydro-1,3-diazepine).[13]

reaction even in the presence of tunneling.[9,10,21] The observed isotope effects on the porphyrin and azophenine tautomerism, therefore, rather indicate a stepwise pathway (Figure 1a), where the transfer of a single deuterium represents the rate-limiting reaction step in both the HD and the DD reactions. This interpretation is in agreement with theoretical studies.[22–24] Since the stepwise reaction pathway involves an intermediate which is highly polar in the case of azophenine, an attempt was made to corroborate this interpretation by detecting the intermediate via the study of kinetic solvent effects.[11] Unfortunately, the rate constants of the azophenine tautomerism were the same in fairly unpolar chlorinated hydrocarbons and in the more polar benzonitrile.[11] This effect was attributed to a shielding of the reaction center from the solvent by the bulky phenyl groups.

To corroborate this interpretation, we focused our attention on the smaller oxalamidine system (OA, Figures 1d and 2). Evidence of the existence of the oxalamidine tautomerism was obtained some years ago for the ^{15}N-labeled tetraphenyloxalamidine (TPOA, R = phenyl) dissolved in organic solvents.[12] Unfortunately, TPOA formed various conformers with differing properties, making it difficult to study the intramolecular tautomerism. The idea therefore arised to stabilize the conformer capable of the intramolecular tautomerism by embedding oxalamidine in bicyclic structures, as shown in Figure 2. Unfortunately, the five-membered derivatives bis(imidazolyl)(BIM) and 2,2′-bis-(4,5-dihydro-1,3-diazole)(OA5) (Figure 2) were not soluble in organic solvents nor subject to a solid-state proton transfer, as checked by high-resolution, solid-state ^{15}N NMR spectroscopy. We therefore prepared the ^{15}N-labeled derivatives OA6 and OA7,

which were soluble in organic solvents. Much to our surprise, OA6 showed no sign of the expected intramolecular double proton transfer shown in Figure 2. As described recently in a preliminary report,[13] the process was, however, detected in OA7 dissolved in methylcyclohexane or acetonitrile; not only kinetic HH/HD/ DD isotope effects but also substantial solvent effects were observed at 362 K. Both effects indicated a stepwise reaction pathway.[13]

In the meantime, we have studied the tautomerism of OA7, including kinetic isotope and solvent effects in a large temperature range using ^{1}H and ^{13}C NMR line-shape analyses and magnetization-transfer experiments. The results of these studies are reported in this paper, together with those obtained for OA6. In addition, we report the syntheses of various [15]N- and [2]H-labeled oxalamidines. Finally, we discuss the mechanism of the oxalamidine tautomerism, which can be derived from the experimental details, in comparison to other proton-transfer systems.

Experimental Section

Synthesis of Isotopically Labeled OA6 and OA7 and Their Precursors. General. As stated above, OA6 and OA7 had to be labeled with the ^{15}N isotope in order to obtain kinetic data by NMR. In the initial stage of our studies on OA7, we also found it convenient to deuterate this molecule in the carbon sites in order to simplify the ^{1}H NMR spectra. The desired isotopically labeled molecules were prepared from the nonlabeled dimethyl ester of ethanediimidic acid (1) and isotopically labeled diamines by modifying the procedure of Weidinger and Kranz,[25] as shown in Figure 3a. We opted for this route, as the direct synthesis from cyanogen and diamines[26] did not give satisfactory results in a small-scale synthesis. The ^{15}N-labeled diamines $H_2^{15}N$-$(CL_2)_n$-$^{15}NH_2$, L = H, D, were synthesized according to Figure 3b. The diamine with n = 4 was prepared via Hofmann degradation[27,28] of $H_2^{15}N$-CO-$(CL_2)_n$-CO-$^{15}NH_2$ obtained from the corresponding acids using [15]NH₄Cl (Chemotrade, Leipzig) as starting material. The diamine with n = 3 was synthesized by Gabriel synthesis[29–32]

(21) Bigeleisen, J. *J. Chem. Phys.* **1955**, *23*, 2264.

(22) Sarai, A. *J. Chem. Phys.* **1982**, *76*, 5554; **1984**, *80*, 5321.

(23) Smedarchina, Z.; Siebrand, W.; Zerbetto, F. *Chem. Phys.* **1989**, *136*, 285.

(24) Merz, K. M.; Reynolds, C. H. *J. Chem. Soc., Chem. Commun.* **1988**, 90. Holloway, M. K.; Reynolds, C. H.; Merz, K. M., Jr. *J. Am. Chem. Soc.* **1989**, *111*, 3466.

(25) Weidinger, H.; Kranz, J. *Chem. Ber.* **1964**, *97*, 1599.

(26) Matsuda, K. U.S. Patent 2.819.262, 1957.

(27) Houben-Weyl, G. Thieme Verlag: Stuttgart, New York, 1957; Vol. 11.1, p 853 ff.

(28) Oxley, P.; Short, W. F. *J. Chem. Soc.* **1947**, 497.

(29) Gabriel, S.; Weiner, J. *Chem. Ber.* **1988**, *21*, 2669.

(30) Putochin, N. *Chem. Ber.* **1926**, *59*, 625.

(31) Int. Minerals & Chem. Corp. U.S. Patent 2.757.198, 1953.

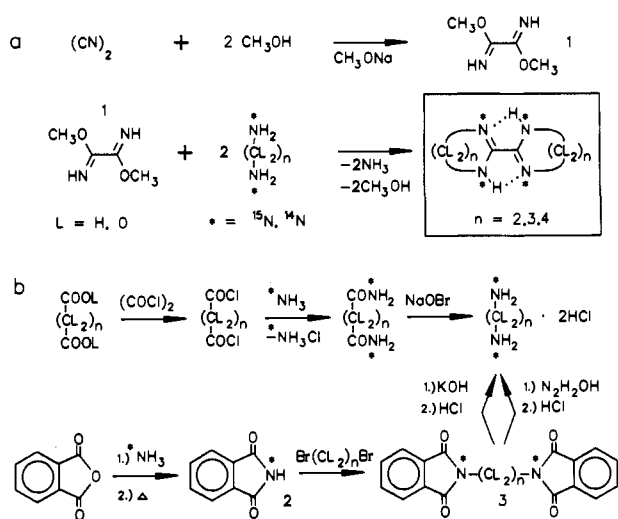(32) Ott, D. G. *Syntheses with Stabile Isotopes*; Wiley: New York, 1981; p 111.

Figure 3. Syntheses of bicyclic, isotopically labeled oxalamidines. Asterisks indicate ^{15}N labels.

from Cl–(CL$_2$)$_3$–Cl and phthalimide-^{15}N (2) with a subsequent alkaline degradation of the alkylenphthalimide-^{15}N (3).[30]

1,3-Diphthalimidopropane-$^{15}N_2$ (3) was prepared by modification of a synthesis given in the literature.[29–31] Phthalimide-^{15}N (2) (3.86 g, 26 mmol) synthesized according to ref 32, potassium carbonate (1.93 g, 14 mmol), dried *in vacuo* at 130 °C for 2 h and 1,3-dibromopropane (1.46 mL, 2.9 g ≡ 14 mmol) were heated for 3 h in 6 mL of dry dimethylformamide over 4-Å molecular sieves. The bath temperature was raised from 130 °C to 190 °C until refluxing started. The reaction mixture was then stirred at room temperature for 12 h. After addition of 50 mL H$_2$O and stirring of the mixture for 1.5 h, the precipitate was filtered and washed with small amounts of methanol and ether to remove 1-bromo-3-phthalimidopropane to give 3.45 g (80%) of 3 with a fp of 200.3 °C (lit.[29] fp 197–198 °C; lit.[30] fp 197 °C).

1,3-Diaminopropane-$^{15}N_2$ (4) was prepared by modification of a synthesis given in the literature.[30] One gram (3 mmol) of 3 was stirred into a solution of 1.4 g (24 mmol) of potassium hydroxide in 4 mL of H$_2$O for 48 h at room temperature until a clear solution resulted. The latter was distilled until dryness into 0.5 mL of concentrated aqueous HCl. After the solution was cooled to room temperature, 10 mL of H$_2$O was added to the residue, and it was again distilled to dryness. This procedure was repeated twice. Removal of the water gave 335 mg (76%) of the hydrochloride of 4 as a colorless salt with a fp of 232 °C (lit.[33] fp 246–250 °C).

To obtain the free diamine, 2.28 mmol of diaminodihydrochloride was stirred for 1 h in a solution of 155 mg (6.75 mmol) of sodium in 2 mL of methanol. The entire solution was evaporated *in vacuo* at 120 °C and recondensed to give a solution of the free diamine 4 in methanol used without isolation for the reaction with 1. The yield of 4 was determined by NMR and/or gas chromatography to be between 70% and 98%.

Adipic Acid Diamide-$^{15}N_2$-d_8 (5) was prepared by modification of a synthesis given in the literature.[32] To avoid possible deuterium losses in the carbon positions, 1.56 g (10 mmol) of adipic acid-d_{10} (a gift of H. Zimmermann, Heidelberg) was dissolved in 4 mL of D$_2$O and stirred for 0.5 h. The solvent was removed and the acid dried *in vacuo* for 24 h (fp 152 °C; lit.[34] fp 153 °C). The acid was dissolved under nitrogen in 10 mL of dry dichloromethane. Oxalyl chloride (3.61 mL, 5.3 g, 42 mmol) and 0.05 mL of *N,N* dimethylformamide were added and stirred at 0 °C for 0.5 h, at room temperature for 2 h, and finally at 60 °C for 0.5 h until the gas evolution ceased. The solvent and oxalyl chloride were removed *in vacuo*, and 8 mL of dichloromethane was added and removed in a similar way. Dry ether (50 mL) was added to the reaction mixture, which was then filtered under nitrogen. Fifty millimoles of ^{15}NH$_3$ gas was condensed into the mixture, which had been cooled to –40 °C. The mixture was allowed to warm up slowly, and HCl gas was added to precipitate nonreacted ^{15}NH$_3$ as the hydrochloride. The reaction mixture was filtered under nitrogen, and the residue was washed with 30 mL of dry ether, dried *in vacuo*, washed twice with 7 mL of cold H$_2$O, and recrystallized twice from 10 mL of H$_2$O to give, after drying, 880 mg

(57%) of 5 with a fp of 216 °C (lit.[34] fp 220 °C). From the unified aqueous phases, nonreacted ^{15}N could be obtained to about 98% as ^{15}-NH$_4$Cl.[32]

1,4-Diaminobutane-$^{15}N_2$-d_8 (6) was prepared by modification of a synthesis given in the literature.[28] To a solution of 0.74 mL (2.3 g, 14.3 mmol) of bromine and 4.1 g (71.4 mmol) of potassium chloride in 15 mL of water was added 880 mg (5.7 mmol) of freshly prepared at 0 °C, pulverized diamide 5, and the solution stirred at 0 °C for 3 h and then refluxed for 3 h. After vapor distillation, the distillate (ca. 2.5 L) was treated with hydrochloric acid. After removal of the solvent, 756 mg of the hydrochloride was obtained.

2,2'-Bis(3,4,5,6-tetrahydro-1,3-diazine) (OA6) was prepared by modification of a synthesis given in the literature.[25] A mixture of 0.5 g (4.3 mmol) of 1, 0.43 g (0.48 mL, 5.8 mmol) of 1,3-diaminopropane, and 4 mg of *p*-toluenesulfonic acid was heated for 1 h to 60 °C. The reaction mixture, which crystallized under NH$_3$ evolution, was filtered and recrystallized from methyl acetate to give 266 mg (1,6 mmol, 55% theoretical yield) of OA6 in the form of colorless twinned needles with a fp of 176.3 °C (lit.[25] fp 170–172 °C).

2,2'-Bis(3,4,5,6-tetrahydro-1,3-diazine)-$^{15}N_4$ (OA6-$^{15}N_4$) had to be prepared in a slightly different way as compared to the unlabeled compound. To a solution of 2.25 mmol of 1,3-diaminopropane-$^{15}N_2$ (4) in 5 mL of methanol were added 140 mg (1.2 mmol) of 1 and 1 mg of *p*-toluenesulfonic acid, and the mixture was stirred in a dry atmosphere for 2 h at 65 °C. The solvent was removed *in vacuo* and the residue treated with 5 mL of chloroform and 1 mL of H$_2$O. The chloroform phase was filtered over basic alumina and the solvent removed *in vacuo* to give 100 mg (53%) of OA6 (fp 170 °C) after recrystallization from methyl acetate.

2,2'-Bis(4,5,6,7-tetrahydro-1,3-diazepine) (OA7) was prepared by modification of a synthesis given in the literature.[25] A solution of 0.46 g (4 mmol) of 1 and 0.8 mL (0.7 g, 8 mmol) of 1,4-diaminobutane in 35 mL of methanol was stirred for 1.5 h at 0 °C and refluxed for 48 h. The methanol was removed, diluted with 10 mL of H$_2$O, and extracted four times with 15 mL of ether. The pale yellow etheric phase was then filtered over a short column filled with basic alumina and evaporated to give 0.52 g (68%) of raw OA7 with a fp of 85 °C (lit.[26] fp 83–90 °C). For further purification, the raw product was dissolved in dry ether and filtered, and the OA7 hydrochloride was precipitated with HCl gas. The precipitate was collected, dissolved in 8 mL of H$_2$O, and treated with potassium hydroxide. After subsequent extraction with ether and evaporation, the purified oxalamidine was recrystallized from the same solvent to give 0.49 g (63%) of OA7, fp 91 °C (lit.[26] 90–92 °C), colorless needles: IR (KBr) 3300, 3240, 2930, 2830, 1650 (w), 1480, 1450 (s), 1435 (s), 1360, 1335, 1275, 1200, 1175 cm^{-1}; MS *m/z* (relative intensity) 195 (13.1), 194 (100), 193 (11.7). Anal. Calcd for C$_{10}$H$_{18}$N$_4$ (194): C, 61.85; H, 9.28; N, 28.87. Found: C, 61.79; H, 9.25; N, 28.96.

2,2'-Bis(4,5,6,7-tetradeuterio-1,3-diazepine)-$^{15}N_4$-d_{16} (OA7-$^{15}N_4$-d_{16}) had to be prepared in a slightly different way as compared to the unlabeled compound. Under a dry nitrogen atmosphere, 172 mg (1.55 mmol) of 1 was added to a solution of 3.1 mmol of 1,4-diaminobutane-$^{15}N_2$ (6) in 5 mL of methanol. The mixture was stirred at 0 °C for 1.5 h and refluxed for 48 h. Gaseous NH$_3$ was removed by repeated gentle flushing with nitrogen gas. The reaction mixture was then treated as in the case of the unlabeled material to give 186 mg (0.87 mmol, 56% theoretical yield) of labeled OA7. The deuterium fraction of 96% in the carbon sites was found by NMR to be the same as in the precursor. A mass spectrum indicated a total ^{15}N fraction of 88.5%.

2,2'-Bis(4,5,6,7-tetrahydro-1,3-diazepine)-$^{15}N_4$ (OA7-$^{15}N_4$) was prepared in analogy to the deuterated material: MS *m/z* (relative intensity) 199 (12.52), 198 (M$^+$, 100), 197 (23.84); isotope analysis, ^{15}N fraction of 88.5%.

Sample Preparation. The NMR samples had to be prepared very carefully in order to avoid acid and basic impurities, especially water which catalyzes undesired intermolecular proton exchange processes. For this purpose, vacuum methods previously described were applied.[5,9] The NMR tubes were sealed to Teflon needle valves, enabling the vacuum transfer of solvents. Acetonitrile-d_3 (AN) was dried over molecular sieves (Merck, 3 Å) and potassium carbonate, methylcyclohexane-d_{14} (MCY) over sodium/potassium alloy with anthracene as an indicator. In the first stage, the substrates were dissolved in acid-free dichloromethane and filtered over a small column with basic alumina into the NMR tube. The latter had been previously treated with aqueous potassium carbonate

(33) Pouchert, C. J. The Aldrich Library of FT-IR-Spektra; Aldrich Co., Inc.: Milwaukee, WI, 1985; Vol. 1, p 1.

(34) Weast, Robert C. *CRC Handbook of Chemistry and Physics*; CRC Press, Inc.: Boca Raton, FL, 1980; p 61.

NMR Study of the Tautomerism of Bicyclic Oxalamidine

J. Am. Chem. Soc., Vol. 116, No. 4, 1994 1233

Table 1. Chemical Shifts of Cyclic Oxalamidines in Different Solvents[a]

compound	solvent	C	T/K	i	δ_i/ppm
OA6-$^{15}N_4$-H$_2$	MCY	0.026	298	1H	6.25
OA6-$^{15}N_4$-H$_2$	MCY	0.026	298	4H	3.285
OA6-$^{15}N_4$-H$_2$	MCY	0.026	298	5H	~1.65
OA6-$^{15}N_4$-H$_2$	MCY	0.026	298	6H	3.144
OA7-H$_2$	MCY	0.485	298	1H	7.267
OA7-HD	MCY	0.536	298	1H	7.270
OA7-$^{15}N_4$-H$_2$	MCY	0.096	298	1H	7.260
OA7-$^{15}N_4$-d_{16}-H$_2$	MCY	0.046	298	1H	7.224
OA7-$^{15}N_4$-d_{16}-HD	MCY	0.060	298	1H	7.214
OA7-$^{15}N_4$-H$_2$	AN	0.049	298	1H	7.114
OA7-$^{15}N_4$-HD	AN	0.044	298	1H	7.104
OA7-$^{15}N_4$-d_{16}-H$_2$	AN	0.007	298	1H	7.070
OA7-$^{15}N_4$-d_{16}-H$_2$	AN	<0.001	298	1H	7.070
OA7-$^{15}N_4$-d_{16}-HD	AN	0.021	298	1H	7.060
OA7-$^{15}N_4$-d_{15}-H$_2$	MCY	0.046	272	4H	3.310
OA7-$^{15}N_4$-d_{15}-H$_2$	MCY	0.046	272	7H	2.827
OA7-$^{15}N_4$-d_{15}-D$_2$	MCY	0.060	270	4H	3.310
OA7-$^{15}N_4$-d_{15}-D$_2$	MCY	0.060	270	7H	2.817
OA7-$^{15}N_4$-H$_2$	AN	0.049	272	4H	3.395
OA7-$^{15}N_4$-H$_2$	AN	0.049	272	7H	2.980
OA7-$^{15}N_4$-D$_2$	AN	0.044	270	4H	3.395
OA7-$^{15}N_4$-D$_2$	AN	0.044	270	7H	2.972
OA7-H$_2$	MCY	0.485	315	4C	51.89
OA7-H$_2$	MCY	0.485	315	5C	31.47
OA7-H$_2$	MCY	0.485	315	6C	30.86
OA7-H$_2$	MCY	0.485	315	7C	46.01
OA7-D$_2$	MCY	0.536	315	4C	51.90
OA7-D$_2$	MCY	0.536	315	5C	31.47
OA7-D$_2$	MCY	0.536	315	6C	30.81
OA7-D$_2$	MCY	0.536	315	7C	45.89

[a] C, concentration in mol L^{-1}; D, deuterium fraction in the mobile proton sites.

Table 2. Coupling Constants in Isotopically Labeled Oxalamidines

compound	n	i	j	$^nJ_{ij}$/Hz
OA6-$^{15}N_4$-H$_2$	1	1H	1N	-93
OA6-$^{15}N_4$-H$_2$	4	1H	3'N	1.6
OA6-$^{15}N_4$-H$_2$	3	1H	6H	2.5
OA6-$^{15}N_4$-H$_2$	3	5H	6H	5.8
OA6-$^{15}N_4$-H$_2$	3	4H	5H	5.8
OA7-^{15}N-d_{15}-H$_2$	1	1H	1N	-82.5
OA7-$^{15}N_4$-d_{15}-H$_2$	4	1H	3'N	2.4
OA7-$^{15}N_4$-d_{15}-H$_2$	3	1H	7H	2.9
OA7-H$_2$	1	7H	7C	136
OA7-H$_2$	1	4H	4C	136
OA7-H$_2$	1	5H	5C	126
OA7-H$_2$	1	6H	6C	126
OA7-$^{15}N_4$-H$_2$	1	7C	1N	8.2

Figure 4. 300.13-MHz ^{1}H NMR signals of OA6-$^{15}N_4$ in methylcyclohexane-d_{14} (MCY) at 298 K. 1.8-μs 35° pulses; 3.8-s repetition time; 2.5-kHz spectral width; 16K spectra; 300 scans; resolution enhancement by line broadening, -1.5; and Gaussian multiplication, 0.3.

solution for 3 days, washed with methanol, and dried. The NMR tube was then attached to the vacuum line, where the solvent was evaporated. Further traces of water in the samples were removed by repeated condensing and evaporating of the dry deuterated solvent into and from the NMR tube.

For deuteration of the NH sites, 0.3 mL of a mixture of CH$_3$OH and CH$_3$OD with the desired deuterium fraction in the mobile proton sites was condensed into the NMR tube containing the dry solid substrate. The mixture was allowed to equilibrate at room temperature for 0.5 h, and then the solvent was evaporated. This procedure was repeated three times. Traces of water and methanol were then removed as described above. During the last stage, 0.5 mL of the desired purified deuterated solvent—determined by means of capillary tubes attached to the vacuum line—was condensed into the NMR tube, which was then removed from the vacuum line by flame sealing, under cooling of its contents down to 77 K.

NMR Measurements. The NMR measurements were performed on a pulse FT NMR spectrometer Bruker MSL 300 (300 13-MHz ^{1}H frequency). The accuracy of the sample temperatures was ±0.4 °C, the temperature constancy ±0.2 °C. ^{13}C NMR spectra were obtained by WALTZ-16 decoupling with under 1 W of power.[35] ^{13}C magnetization-transfer experiments in the rotating frame[7] were obtained using the usual pulse sequence,[7,11] employing in this case permanent Waltz-16 ^{1}H decoupling. Since the longitudinal relaxation times in the rotating frame may be affected by decoupling, the decoupling power[36] was minimized in such a way that the same results were obtained for permanent and gated WALTZ-16 decoupling. The reported chemical shifts are referenced to external TMS as usual. The NMR spectra were transferred to a personal computer, where the line shapes were simulated using homemade programs[5] based on those of Binsch.[37,38] For data analyses, nonlinear least-squares fitting routines were employed.[39]

(35) Shaka, A. J.; Keeler, J.; Frenkiel, T.; Freeman, Ray *J. Magn. Reson.* **1983**, *52*, 335.

(36) Doddrell, D. M.; Bendall, M. R. *Chem. Commun.* **1979**, *2*, 77. Deverell, C.; Morgan, P. E.; Strange, J. H. *Mol. Phys.* **1970**, *18*, 553.

(37) Binsch, G. *J. Am. Chem. Soc.* **1969**, *91*, 1304.

(38) Kleier, A.; Binsch, G. *QCPE* **1969**, *140*.

(39) Marquardt, D. W. *Share Distribution Center* 1964, revised program 1428.

Results

In this section we describe the results of the dynamic NMR experiments performed on OA6 and OA7 dissolved in various solvents. In the following, nuclei are numbered according to the position in the molecular skeleton and the type, e.g., 1H refers to the hydrogen atom in position 1. The chemical shift of 1H is expressed by the symbol ν_{1H} and the scalar coupling constant between 1H and 1N by $^1J_{1H1N}$, where N refers to the ^{15}N isotope. Chemical shifts and coupling constants are assembled in Tables 1 and 2. All parameters of the line shape analyses performed are assembled in Tables 4 and 5 of the supplementary material.

^{1}H NMR Spectroscopy of OA6 in Methylcyclohexane-d_{14} (MCY). The room temperature ^{1}H NMR spectrum of OA6 in MCY is shown in Figure 4. Only the signals of the mobile protons 1H, 4H, and 7H are shown, the signal of 5H being covered by the solvent peak. The spectral analysis is straightforward. The signal of the mobile protons 1H is split by coupling with 1N into a doublet with $^1J_{1H1N}$ = -82.5 Hz. The negative sign arises from the negative gyromagnetic ration of ^{15}N.[40] Each line is further split into a doublet by coupling with the ^{15}N atom in the 3' position. This assignment and the positive sign of the corresponding coupling constant do not result directly from the spectrum in Figure 4 but rather from arguments discussed below in the case of OA7. Each line component of the 1H signal is further split into four barely resolved triplets arising from coupling with 6H$_a$ and 6H$_b$. The signals of 5H and 6H consist of triplets where the line components of 6H are split into doublets by coupling with 1H. In other words, the two protons a and b in each of the CH$_2$ groups are not only chemically equivalent but also quasi-magnetically equivalent within the margin of error. The chemical equivalence is the result of fast ring dynamics. The magnetic equivalence is not an intrinsic feature but rather is caused by similar values of the vicinal coupling

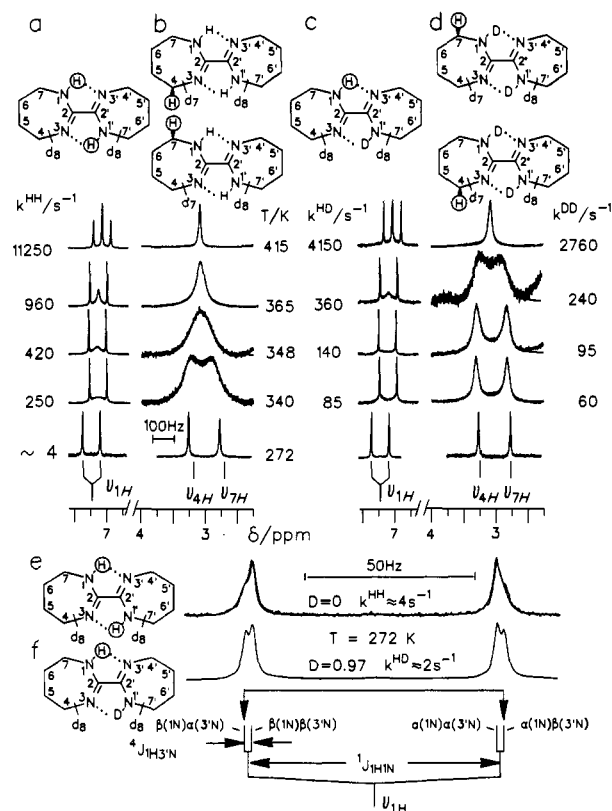(40) Witanowski, M.; Webb, G. A. *Nitrogen NMR*; Plenum Press: London, New York, 1973; p 262ff.

Figure 5. Superposed experimental and calculated 300.13-MHz ^{1}H NMR signals of ^{15}N-labeled OA7 dissolved in methylcyclohexane-d_{14} (MCY) as a function of temperature and the deuterium fraction D in the mobile proton sites. The compound was deuterated in the carbon sites. 1000–10 000 scans, otherwise experimental conditions as in Figure 4. Column a: $D = 0$, $C = 0.046$ mol L^{-1}. Columns c and d: $D = 0.97$, $C = 0.06$ mol L^{-1}. Rows e and d: expanded $1H$ signals at 272 K and $D = 0$ and at $D = 0.97$. The signals stem predominantly from the encircled proton sites of the associated OA7 isotopomers: OA7-$^{15}N_4$-d_{16}-HH (a and e), OA7-$^{15}N_4$-d_{15}-HH (b), OA7-$^{15}N_4$-d_{16}-HD (c and f), OA7-$^{15}N_4$-d_{15}-DD (d). Minor contributions: OA7-$^{15}N_3$-d_{16}-HH (a and e), OA7-$^{15}N_3$-d_{16}-HD (c and f), OA7-$^{15}N_4$-d_{15}-HD (d). For further explanation, see text.

constants in the cis and the trans forms, which is consistent with the literature.[41]

In the temperature range between 280 and 410 K, no spectral changes were observed which could stem from intramolecular or intermolecular proton-transfer processes. An idea about the minimal activation energy of the intramolecular tautomerism of OA6 can be obtained as follows. Assuming a frequency factor of $A^{HH} \approx 10^{11.5}$ s^{-1} found below for the tautomerism of OA7 and a normal Arrhenius law, it follows, with a rate constant of k^{HH} < 1 s^{-1} at $T = 410$ K, that $E_a^{HH} > 90$ kJ mol^{-1}.

^{1}H NMR of OA7 in Methylcyclohexane-d_{14} (MCY). To simplify the line shape analyses in the initial stages of this work, OA7 was not only enriched with ^{15}N but also deuterated in the carbon sites. Some typical superposed experimental and calculated ^{1}H NMR signals of this isotopomer dissolved in MCY are shown in Figure 5 as a function of temperature, at two deuterium fractions of $D = 0$ and 0.97 in the mobile proton sites. The various signals dominantly stem from the circled positions of the associated isotopomers in Figure 5. Therefore, the line shapes in Figures 5a and 5b depend on the rate constant k^{HH}, those of Figure 5c on k^{HD}, and those of Figure 5d on k^{DD}.

The signals of 4H and 7H constitute singlets at low temperatures, where hydrogen transfer is slow. The lines are slightly broadened by unresolved couplings with vicinal deuterons. At D = 0, the 7H signal is further broadened by an unresolved scalar

(41) Karplus, M. *J. Chem. Phys.* **1959**, *30*, 11. Karplus, M. *J. Am. Chem. Soc.* **1963**, *85*, 2870.

coupling with 1H. This coupling was later resolved when a sample of OA7-$^{15}N_4$-HH was studied. As temperature is increased, both signals broaden and coalesce; the coalescence temperature is higher at $D = 0.97$ as compared to $D = 0$ because k^{DD} is smaller than k^{HH}.

At low temperatures, the 1H signals are split by coupling with 1N into doublets. As shown in the expanded spectra set of Figures 5e and 5f, each line component is further split into barely resolved doublets, indicating a long-range coupling to another ^{15}N atom as in the case of OA6. This atom can easily be identified by line shape analysis using arguments described previously;[5] e.g., in the case of a long-range coupling of 1H with 3'N, i.e., the atom to which it jumps, a pure triplet is expected in the fast proton exchange regime as observed experimentally in Figures 5a and 5c; the high- and low-field components of the triplets stem from the molecules where the two nitrogen neighbors are in the spin states $\alpha(1N)\alpha(3'N)$ and $\beta(1N)\beta(3'N)$. The center line stems from the molecules where the two nitrogen neighbors are either in spin state $\alpha(1N)\beta(3'N)$ or in $\beta(1N)\alpha(3'N)$. If 1H were additionally coupled with either 3N or 1'N, a triplet should also appear at high temperature because 1H is now equally bound to 1N and to 3'N, but each triplet line component should be further split into subtriplets arising from average scalar coupling to 3N and 1'N. This is obviously not the case.

The assignment of the nitrogen spin states to the line components shown in Figures 5e and 5f is straightforward. As illustrated in Figures 5a, 5c, 5e, and 5f, the line components with the frequencies $\nu_{1H} + (^1J_{1H1N} - {}^3J_{1H3'N})/2$ and $\nu_{1H} - (^1J_{1H1N} - {}^3J_{1H3'N})/2$ are not modulated by the proton transfer, i.e., they stem from the protons jumping between nitrogen pairs in the spin states $\alpha(1N)\alpha(3'N)$ and $\beta(1N)\beta(3'N)$. By contrast, the lines absorbing at $\nu_{1H} + (^1J_{1H1N} - {}^3J_{1H3'N})/2$ and $\nu_{1H} + (-^1J_{1H1N} + {}^3J_{1H3'N})/2$ broaden and coalesce as the proton transfer becomes fast. These lines, therefore, stem from the protons jumping between ^{15}N pairs in the spin states $\alpha(1N)\beta(3'N)$ or $\beta(1N)\alpha(3'N)$. This assignent implies that $^3J_{1H3'N}$ is positive since $^1J_{1H1N}$ is negative.

The spectra in Figure 5a could then be simulated without assumptions. From the line components not affected by the exchange, the line widths in the absence of exchange could be extracted at each temperature. The rate constants k^{HH} were obtained by simulating the signal components affected by exchange broadening and coalescence. A small amount (11.5%) of the isotopomer OA7-$^{15}N_3$-d_{16} was taken into account during the simulations in a similar way to the way described previously.[5] Using the obtained values of k^{HH}, it was then possible to simulate the 4H/7H signals in Figure 5b using simple two-site theory by adapting the line width in the absence of exchange. The values of the chemical shifts ν_4 and ν_7 were obtained by simulation in the slow exchange regime and were taken in the fast exchange regime from the spectra at D = 0.97, after a minor correction for the H/D isotope effect on ν_4 and ν_7. In the next stage, the 4H/7H signals at D = 0.97 were simulated using the same static parameters by adapting only the rate constant k^{DD} (Figure 5d). Finally, the 1H signals of Figure 5c were simulated in a similar way as in Figure 5a by adapting k^{HD}. In addition, a small amount (3%) of the isotopomer OA7-$^{15}N_4$-d_{16}-HH was taken into account.

^{13}C NMR of OA7 in MCY. To increase the precision of the kinetic data set, we performed ^{13}C NMR experiments on unlabeled OA7 dissolved in MCY. The superposed experimental and simulated ^{1}H-decoupled ^{13}C NMR signals of the carbon pairs 4C/7C and 5C/6C are shown in Figure 6 as a function of temperature at D = 0 and 0.99. At low temperature, each carbon site contributes a singlet to the spectra. The assignment is straightfoward. Proton transfer leads to line broadening and coalescence within each signal pair. The coalescence temperature is lower for the pair 5C/6C than for the pair 4C/7C because of the smaller chemical shift difference. The signal of 2C could not be observed, probably because of very long longitudinal relaxation
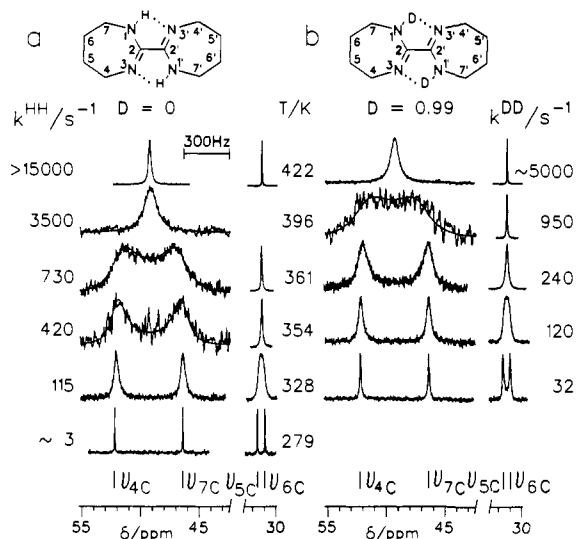
Figure 6. Superposed experimental and calculated 75.468-MHz ^{13}C NMR spectra of OA7 in MCY. (a) $D = 0$, $C = 0.485$ mol L^{-1}; (b) $D = 0.99$, $C = 0.536$ mol L^{-1}. WALTZ decoupling <1 W;[35] 60° pulses; 3.8–5-s repetition time; 1000–20 000 scans.

times. At low temperatures, proton-coupled carbon spectra were taken, from which the coupling constants assembled in Table 2 were obtained. The line shape changes observed were calculated in terms of the usual two-site theory. Both the 4C/7C and the 5C/6C signals were fitted simultaneously.

In the low-temperature range, ^{13}C NMR magnetization-transfer experiments in the rotating frame were performed on the signals 7C and 4C as described in the Experimental Section. A typical experiment is shown in Figure 7. In the "parallel" experiments of Figures 7a and 7c, the signal decays are governed by the inverse longitudinal relaxation times in the rotating frame, $1/T_{1\rho}$, in the "antiparallel" experiments of Figures 7b and 7d by $1/T_{1\rho} + 2k^{HH}$ at $D = 0$ and by $1/T_{1\rho} + 2k^{DD}$ at $D = 0.97$. Exponential decays were obtained in all cases as illustrated in Figure 7e. The kinetic HH/DD isotope effect is well pronounced. The rate constants obtained in this way were used to adapt the line width in the absence of exchange in the line shape analyses of Figure 6 at low temperatures. These widths were then kept constant in the simulation of the spectra obtained at higher temperatures.

NMR Spectroscopy of OA7 in Acetonitrile-d_3 (AN). Due to solubility problems, only ^{1}H NMR experiments could be performed on solutions of OA7 in AN. During the high-temperature measurements, a partial deuteration of the title compound in the mobile proton sites by the solvent was observed. Since the time required for obtaining good signal-to-noise ratios for the 4H/7H signals was much shorter for OA7-$^{15}N_4$ as compared to OA7-$^{15}N_4$-d_{16}, most ^{1}H NMR experiments were carried out on the former compound in order to minimize the deuteration problems. To obtain simple spectra as shown in Figure 8, which exhibit the same spectral features as those of Figure 5, scalar coupling between 1H and 4H was removed by homodecoupling when the 1H signal was measured. In a similar way, the 4H/7H signals were obtained with the coupling to the 5H/6H removed; however, the residual coupling to 1H remained, leading again to a differential line broadening between the 7H and the 4H signals in the slow exchange regime. The main difference between the spectra of Figures 5 and 8 is that in the latter the coalescence temperatures are significantly lowered because the OA7 tautomerism is faster in AN than in MCY. According to Table 1, there is only very little influence of the solvent on the chemical shifts and the coupling constants.

Kinetic Data of OA7 in MCY and AN. The rate constants obtained did not depend on the method used nor on the
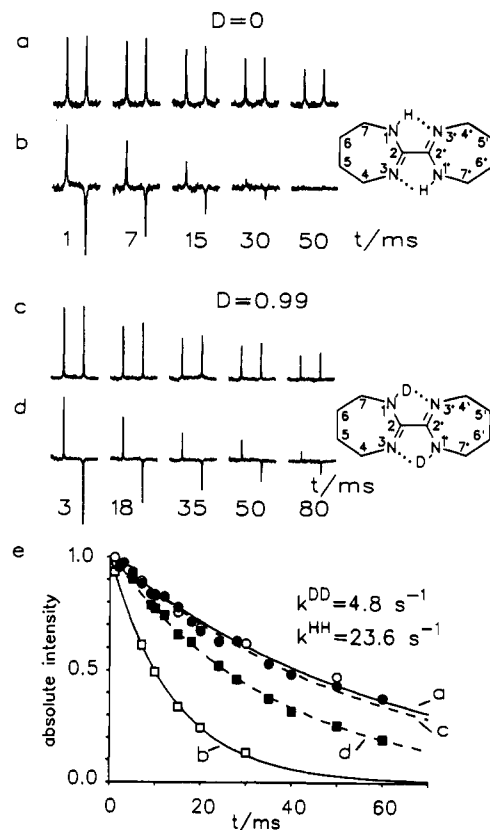

Figure 7. ^{13}C magnetization-transfer experiments in the rotating frame at 302.8 K performed on the 4C/7C positions of OA7 in MCY. (a) $D = 0$, $C = 0.485$ mol L^{-1}, parallel experiment; (b) corresponding antiparallel experiment; (c) $D = 0.99$, $C = 0.536$ mol L^{-1}, parallel experiment; (d) corresponding antiparallel antiparallel experiment; (e) data analysis.
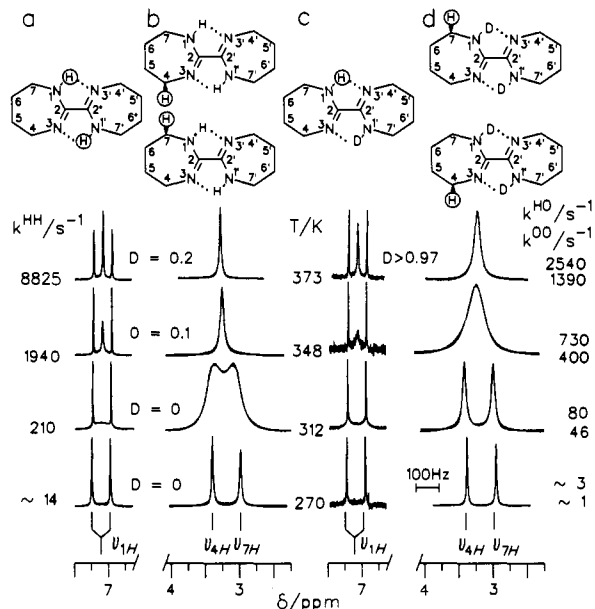

Figure 8. Superposed experimental and calculated 300.13-MHz ^{1}H NMR spectra of ^{15}N-labeled OA7 (nondeuterated in the carbon sites) dissolved in acetonitrile-d_3 (AN) under homodecoupling conditions. 200–10 000 scans, otherwise experimental conditions as in Figure 4. For further explanation, see Figure 5.

concentration nor on isotopic substitution in sites other than the mobile proton sites. Therefore, single Arrhenius curves were constructed as shown in Figure 9. The data assembled in Tables 4 and 5 of the supplementary material can be expressed by the following:
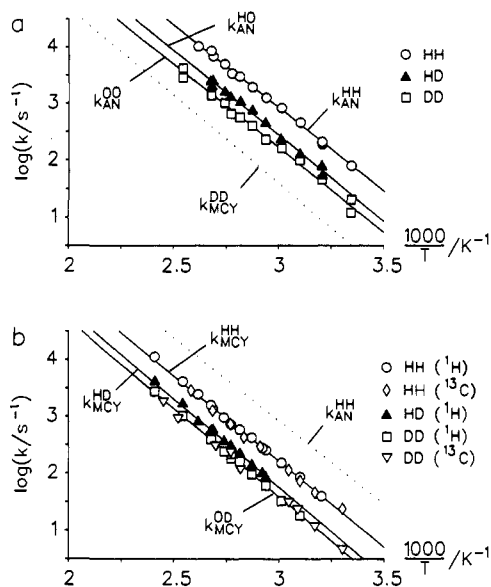
Figure 9. Arrhenius diagram of the tautomerism of OA7. (a) Solvent was acetonitrile-d_3 (AN); (b) solvent was methylcyclohexane-d_{14} (MCY).

$$k_{MCY}^{HH} = 10^{11.24 \pm 0.08} \exp(-57.6 \pm 0.6 \text{ kJ mol}^{-1}/RT) \text{ s}^{-1},$$

$$303 \text{ K} \le T \le 415 \text{ K}, \quad k_{MCY}^{HH}(298 \text{ K}) \approx 13.8 \text{ s}^{-1} \quad (1)$$

$$k_{MCY}^{HD} = 10^{11.10 \pm 0.12} \exp(-59.6 \pm 1.0 \text{ kJ mol}^{-1}/RT) \text{ s}^{-1},$$

$$340 \text{ K} \le T \le 415 \text{ K}, \quad k_{MCY}^{HD}(298 \text{ K}) \approx 4.4 \text{ s}^{-1} \quad (2)$$

$$k_{MCY}^{DD} = 10^{10.9 \pm 0.1} \exp(-59.5 \pm 0.7 \text{ kJ mol}^{-1}/RT) \text{ s}^{-1},$$

$$303 \text{ K} \le T \le 415 \text{ K}, \quad k_{MCY}^{DD}(298 \text{ K}) \approx 2.9 \text{ s}^{-1} \quad (3)$$

$$k_{MCY}^{HH}/k_{MCY}^{HD} \approx 3.1, \quad k_{MCY}^{HH}/k_{MCY}^{DD} \approx 4.8,$$

$$k_{MCY}^{HD}/k_{MCY}^{DD} \approx 1.5 \quad (4)$$

$$k_{AN}^{HH} = 10^{11.72 \pm 0.12} \exp(-56.2 \pm 0.9 \text{ kJ mol}^{-1}/RT) \text{ s}^{-1},$$

$$300 \text{ K} \le T \le 382 \text{ K}, \quad k_{AN}^{HH}(298 \text{ K}) \approx 75.0 \text{ s}^{-1} \quad (5)$$

$$k_{AN}^{HD} = 10^{11.46 \pm 0.06} \exp(-57.6 \pm 1.4 \text{ kJ mol}^{-1}/RT) \text{ s}^{-1},$$

$$312 \text{ K} \le T \le 374 \text{ K}, \quad k_{AN}^{HD}(298 \text{ K}) \approx 23.1 \text{ s}^{-1} \quad (6)$$

$$k_{AN}^{DD} = 10^{11.09 \pm 0.15} \exp(-56.65 \pm 1.2 \text{ kJ mol}^{-1}/RT) \text{ s}^{-1},$$

$$300 \text{ K} \le T \le 393 \text{ K}, \quad k_{AN}^{DD}(298 \text{ K}) \approx 14.5 \text{ s}^{-1} \quad (7)$$

$$k_{AN}^{HH}/k_{AN}^{HD} \approx 3.2, \quad k_{AN}^{HH}/k^{DD} \approx 5.2, \quad k_{AN}^{HD}/k_{AN}^{DD} \approx 1.6 \quad (8)$$

$$k_{AN}^{HH}/k_{MCY}^{HH} \approx 5.4 \text{ at } 298 \text{ K} \quad (9)$$

Discussion

Using various methods of dynamic NMR spectroscopy, we obtained the rate constants and the kinetic HH/HD/DD isotope effects of the tautomerism of OA7 (Figure 2) for two solvents of different polarity. For the first time, substantial kinetic solvent effects were observed for an intramolecular degenerate double proton-transfer reaction. The kinetic HH/HD isotope effects are substantially larger than the kinetic HD/DD isotope effects and are independent of the solvent polarity. No tautomerism could be detected for OA6 (Figure 2). In this section, we show that both kinetic solvent effects and the kinetic isotope effects give evidence of the stepwise, rather than the concerted, reaction pathway illustrated in Figure 1, where substantial solvent and intramolecular heavy atom reorganization precedes the proton transfer. Assuming that the reorganization process consists

mainly of a compression of the proton-transfer units, the observed structural effects on the tautomerism of oxalamidines can thus be modeled.

Kinetic Solvent Effects. From the observation of concentration- and solvent-independent chemical shifts of the mobile protons, it follows that OA6 and OA7 do not form intermolecular hydrogen bonds, neither in methylcyclohexane nor in acetonitrile. Therefore, the rate constants obtained do not contain terms arising from hydrogen bond equilibria preceding the intramolecular proton transfer but refer to the latter process alone. For a concerted proton transfer where two protons are in flight (Figure 1), kinetic solvent effects should be minimal because the solute–solvent interactions are not expected to vary substantially during the course of the reaction. By contrast, solute–solvent interactions are expected to vary substantially during the stepwise reaction pathway if the metastable intermediate is zwitterionic (Figure 1d). In this case, the transition states are also highly polar. This phenomenon should lead to an enhancement of the rate constants in polar solvents.[42–45] The finding that the OA7 tautomerism is 5.4 times faster in acetonitrile at 298 K (AN, dielectric constant $\epsilon = 37.5$) than in methylcyclohexane (MCY, $\epsilon = 2.02$) is therefore a strong evidence for the formation of a metastable zwitterion, i.e., for a stepwise reaction pathway (Figure 1d). We could not find reference data in the literature concerning kinetic solvent effects on intramolecular reactions of neutral nonpolar molecules involving highly polar transition states in order to classify the size of the observed kinetic solvent effects. It is, however, interesting to note that Caldin and Mateo[46] did observe for the proton-transfer reaction

$$AH + B \overset{fast}{\rightleftharpoons} AH\cdots B \overset{slow}{\rightleftharpoons} A^-\cdots HB^+ \overset{fast}{\rightleftharpoons} A^- + HB^+ \quad (10)$$

where AH = (4-nitrophenyl)nitromethane (NPNM) and B = tetramethylguanidine (TMG), a kintic solvent effect of the same order, i.e. $k(AN)/k(CY) \approx 3$, where CY represents cyclohexane ($\epsilon = 2.02$). Thus, the expectation of larger kinetic solvent effects for the formation of ion pairs or zwitterions from neutral initial states than found here is not realistic. In the case of the OA7 tautomerism, the solvent effect is caused by both a decrease of the activation entropy $\Delta H^\ddagger(AN) - \Delta H^\ddagger(MCY) = -2 \text{ kJ mol}^{-1}$ and an increase of the activation entropy $\Delta S^\ddagger(AN) - \Delta S^\ddagger(MCY) = 7 \text{ J K}^{-1} \text{ mol}^{-1}$ when MCY is replaced by AN. In the NPNM + TMG reaction, both contributions are larger, i.e., $\Delta H^\ddagger(AN) - \Delta H^\ddagger(CY) = +4.2 \text{ kJ mol}^{-1}$ and $\Delta S^\ddagger(AN) - \Delta S^\ddagger(CY) = 24 \text{ J K}^{-1} \text{ mol}^{-1}$, bu they partly compensate, leading to the smaller overall kinetic solvent effect. The entropy changes in both cases can easily be understood in terms of solvent ordering during the proton transfer, which is more pronounced in the case of the highly polarizable solvent CY and MCY, whereas in the case of AN, the permanent solvent dipoles are already partially ordered in the initial state. The higher activation energy of the NPNM + TMG reaction in AN as compared to CY could perhaps arise from the formation of weak hydrogen bonds between NPMG and acetonitrile which have to be broken in the initial reaction step.

It follows that the azophenine tautomerism (Figure 1c) should also be only 2–3 times faster in benzontrile ($\epsilon = 25$) as compared to toluene ($\epsilon = 2$). Experimentally, no difference was observed.[11] Since the expected values are so small, it is impossible to state that the experimental observations are not in agreement with the formation of a zwitterion intermediate, as has been discussed previously.[11]

(42) Reichardt, C. *Lösungsmitteleffekte in der Organischen Chemie*; Verlag Chemie: Weinheim, 1988.

(43) Fritsch, J.; Zundel, G. J. *J. Phys. Chem.* **1984**, *88*, 321.

(44) Jain, D. C.; Sapse, A. M.; Cowburn, D. *J. Phys. Chem.* **1988**, *92*, 6847.

(45) Gompper, R. *Angew. Chem.* **1969**, *81*, 348; *Angew. Chem., Int. Ed. Engl.* **1969**, *8*, 312.

(46) Caldin, E. F.; Mateo, S. J. *J. Chem. Soc., Faraday Trans. 1* **1975**, *71*, 1876.
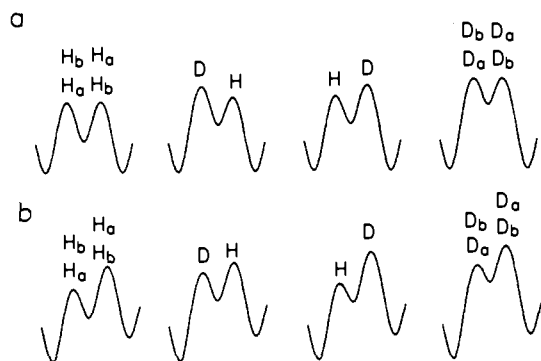
NMR Study of the Tautomerism of Bicyclic Oxalamidine

J. Am. Chem. Soc., Vol. 116, No. 4, 1994 1237

Figure 10. Free energy reaction profiles for reversible stepwise HH/HD/DH/DD transfers involving an intermediate according to Figure 1a. (a) Degenerate case; (b) nondegenerate case.

Kinetic Hydrogen/Deuterium Isotope Effects. General Aspects.

We discuss the observed kinetic isotope effects on the tautomerism of OA7 in terms of the following expressions derived previously[11,14] for the case of a reversible, degenerate, stepwise, double proton-transfer reaction:

$$k^{HH}/k^{HD} = (P + S)/2, \quad k^{HD}/k^{DD} =$$
$$2/(P^{-1} + S^{-1}), \quad k^{HH}/k^{DD} = PS \quad (11)$$

Equation 11 was based only on formal kinetics.[11,14] P is the primary H/D isotope effect of the proton in flight, S the secondary isotope effect caused by the bound mobile proton. S is close to 1 if the binding situation of the bound mobile proton is such that its vibrational frequencies do not change substantially during the course of the reaction. In other words, it follows from eq 11 that *one can directly compare the rate constants k^{HH} and k^{DD} with the rate constants k^{H} and k^{D} of other single proton-transfer reactions.* Equation 11 is depicted in Figure 10a. The reaction profiles of the HH and the DD reactions are symmetric. Either the proton in site a or the one in site b is transferred first. The profile for the transfer of one H and one D is asymmetric, i.e., there is only one rate-limiting step in which the D isotope is transferred. The associated barrier is of the same height as in the DD case; however, the HD reaction is approximately twice as fast as the DD reaction because in the latter there are two rate-limiting barriers of equal height, as expressed by eq 11. In the asymmetric case (Figure 10b), the degeneracy of the HD and the DH reactions is lifted. The HD reaction now becomes as slow as the DD reaction and the DH reaction as fast as the HH reaction.[11,14]

Using eq 11, we calculate from eqs 1–9 the values $P = 5.4$ and $S = 0.88$ for OA7 in methylcyclohexane and $P = 5.6$ and $S = 0.92$ for OA7 in acetonitrile at a temperature of 298 K. Therefore, within the margin of error, the primary isotope effects are the same for both solvents. The finding that S is close to 1 corroborates the stepwise pathway. A closer look at the precision of our data shows that they would also be consistent with values of $S = 1$ in the whole temperature range. Assuming the Arrhenius relations

$$k^{HH} = A^{HH} \exp(E_a^{HH}/RT),$$
$$P = A^{H}/A^{D} \exp(\Delta E/RT) \quad (12)$$

and the validity of eq 11 with $S = 1$, the dependence of all isotopic rate constants k^{HH}, k^{HD}, and k^{DD} on temperature is then only a function of the three parameters A^{HH}, A^{H}/A^{D}, and ΔE. From a free simultaneous fit of all three Arrhenius curves, we obtained values of A^{H}/A^{D} somewhere between 1 and 2, indicating the usual mass effect on vibrations involving hydrogen atoms in the order of 0.7 to $\sqrt{2}$.[47] We therefore fixed A^{H}/A^{D} to $\sqrt{2}$. Moreover, we found that ΔE was identical for the solvents MCY

---

(47) Bell, R. P. *The Tunnel Effect in Chemistry*; Champman and Hall: London, 1980.
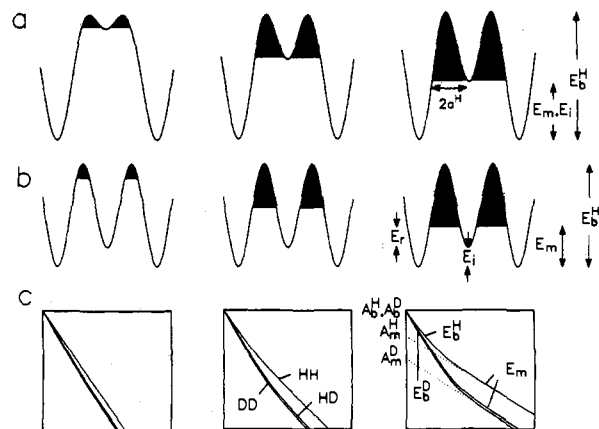

Figure 11. Visualization of a modified Bell tunneling model for degenerate, stepwise double proton transfers involving an intermediate. A minimum energy E_m is required for proton tunneling, which can take place only in the hatched regions. E_b, barrier energy. (a) E_m is given by the energy of the intermediate, E_i (b) E_m is given by $E_i + E_r$, where E_r is associated with heavy atom reorganization preceding the proton transfer. (c) Corresponding Arrhenius curves (schematically) calculated in terms of the modified Bell tunneling model as described in the text.

and AN. The final kinetic results of the tautomerism of OA7 can, therefore, be expressed as

$$A^{HH}(MCY) = 10^{11.2} \text{ s}^{-1}, \quad E_a^{HH}(MCY) =$$
$$57.6 \text{ kJ mol}^{-1} \quad (13)$$

$$A^{HH}(AN) = 10^{11.6} \text{ s}^{-1}, \quad E_a^{HH}(AN) = 55.7 \text{ kJ mol}^{-1} \quad (14)$$

$$\Delta E(MCY) = \Delta E(AN) = 3.2 \text{ kJ mol}^{-1} \quad (15)$$

from which it follows that

$$P_{298 \text{ K}}(MCY) = P_{298 \text{ K}}(AN) = 5.1 \quad (16)$$

The Arrhenius curves calculated using this data set and those shown in Figure 9 calculated by linear regression are difficult to distinguish by the eye.

Size of the Primary Isotope Effects. The size of the primary isotope effect $P_{298 \text{ K}}$ of the OA7 tautomerism is of the magnitude usually found for overbarrier proton-transfer reactions.[47] It is, however, smaller than the value of $P_{298 \text{ K}} \approx 7$ found previously for the azophenine tautomerism[11] (Figure 1c) and the value of $P_{298 \text{ K}} \approx 18$ found for the tautomerism *meso*-tetraphenylporphyrin[6] (Figure 1b). It is evident that these variations are associated with the differing chemical structures, but which structural features are important?

The large value of $P_{298 \text{ K}}$ in the case of the porphyrin tautomerism has been explained in terms of a tunneling model,[19,20] illustrated in Figure 11. The model is based on the model of Bell[47] but involves a minimum energy E_m for tunneling to occur.[6,9] Equilibrium isotope effects between the initial state and the intermediate are neglected. The barrier is represented by an inverted parabola. The calculation of the Arrhenius curves of the HH, HD, and DD reactions taking into account eqs 11 and 12 and neglecting secondary kinetic isotope as well as equilibrium isotope effects between the initial states and the intermediate states is straightforward.[6,9,19,20] These curves depend only on the barrier heights E_b^{L}, L = H,D, the barrier widths $2a^{L}$, the masses of H and D, the minimum energy E_m, and the preexponential factors A_b^{L} for the overbarrier reactions. Within this model, the Arrhenius curves are given in the high-temperature limit by

$$k^{HH} = A_b^{H} \exp(-E_b^{H}/RT), \quad k^{DD} = A_b^{D} \exp(-E_b^{D}/RT) \quad (17)$$

and at low temperatures by

$$k^{HH} = A_m^H \exp(-E_m/RT), \quad k^{DD} = A_m^D \exp(-E_m/RT) \quad (18)$$

Equation 17 represents the overbarrier reaction involving usual kinetic H/D isotope effects. Equation 18 predicts a temperature-independent kinetic isotope effect A_m^H/A_m^D at low temperatures which is much smaller than the values predicted classically in terms of eq 17. However, there is an intermediate temperature range where the isotope effects are larger than predicted classically, as has been discussed by Stern and Weston on the grounds of the Bell tunneling model.[48]

In Figure 11, some typical cases characterized by different reaction profiles of the degenerate, stepwise proton transfers are depicted. In all cases, the total barrier heights for each single reaction step are the same; in addition, it is assumed that the classical kinetic hydrogen/deuterium isotope effects for the overbarrier reactions are the same. Therefore, in the high temperature regime, the associated Arrhenius curves shown in Figure 11c coincide. However, as illustrated in Figure 11c, drastic differences are expected at lower temperatures, when tunneling becomes important. This phenomenon can, however, occur only at energies indicated by the shadowed areas, e.g., in Figure 11a, tunneling cannot occur at energies lower than the energy of the intermediate, E_i, as discussed previously for the porphyrin case.[19,20,22] Thus, reducing the values of $E_m = E_i$ leads to a decrease of the slope of the Arrhenius curves in Figure 11c by moving from the left to the right. Since the total barrier height is kept constant, the shadowed barrier areas increase. It is well known[47] that the low-temperature kinetic isotope effects A_m^H/A_m^D and, consequently, the isotope effects in the total temperature range increase exponentially with the size of the barrier areas. In other words, if tunneling can occur only slightly below the top of the barrier, then A_m^H/A_m^D is much smaller as compared to the case where tunneling can occur at lower energies. This leads to larger kinetic isotope effects in the whole temperature range, as illustrated in Figure 11c.

Additionally, in Figure 5b, a term E_r arising from heavy atom reorganization preceding the proton transfer is assumed. Since the tunneling probabilities are minimal for the heavy atom motions due to the large masses involved, the minimum energy is then given by $E_m = E_i + E_r$, as illustrated in Figure 11b, where E_i is kept constant but E_r is decreased from the left to the right. The associated changes of the isotopic Arrhenius curves are qualitatively similar to those shown in Figure 11a.

In conclusion, the relatively small kinetic H/D isotope effects on the oxalamidine tautomerism can be explained either with a larger energy E_i of the intermediate and/or of the energy E_r required for heavy atom reorganization preceding single proton tunneling, as compared to the porphyrin case. E_i could be larger in oxalamidine because of the charge separation energy necessary for the proton transfer to occur; in addition, E_r may be larger because of the associated solvent reorientation absent in the porphyrin case.

Structural Aspects of the Tautomerism of Oxalamidines. Charge separation and solvent reorganization alone cannot, however, explain why the oxalamidine tautomerism is very slow in OA6, faster in OA7, and relatively fast in TPOA. The question arises as to whether these differences can be explained in terms of a structure-dependent solvent reorganization of the molecular skeleton. Before answering this question, let us first discuss all structural information available about this class of compound.

Experimental Information Concerning the Structure of Oxalamidines. A measure of the strength of intramolecular hydrogen bonding in oxalamidines and azophenine (AP) is provided by the values of the chemical shifts ν_{1H} of the mobile protons. The stronger the hydrogen bond, the larger are the latter. As shown in Figure 12, the hydrogen bond strength correlates well with the energy of activation of the intramolecular tautomerism. The
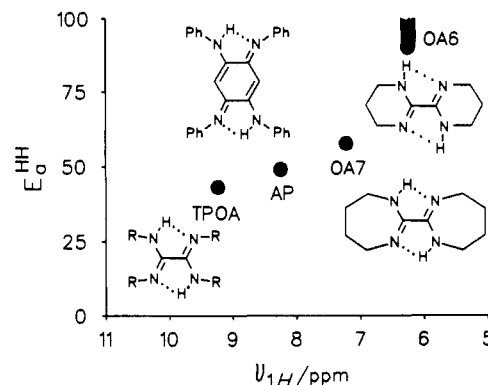
(48) Stern, M. J.; Weston, R. E. *J. Chem. Phys.* **1974**, *60*, 2803.

Figure 12. Experimental energies of activation of the intramolecular double proton transfer in oxalamidines and azophenine as a function of the chemical shift of the mobile protons. The data for TPOA stem from ref 12 and for AP from ref 11.
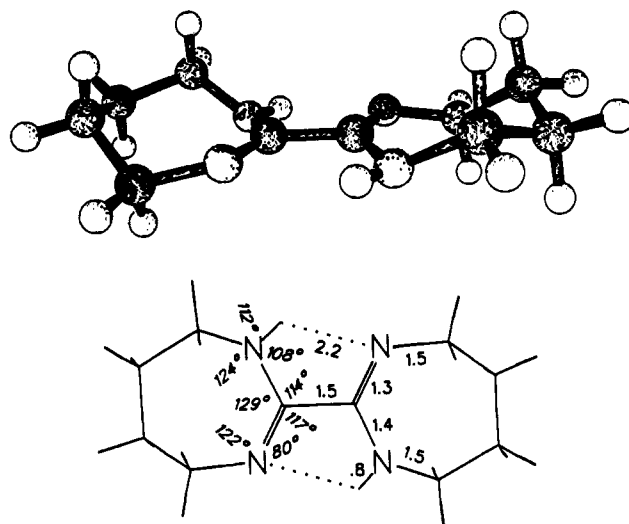

Figure 13. Crystal structure of OA7 according to ref 50.

strongest intermolecular hydrogen bond in this series is formed by TPOA, followed by azophenine, OA7, and OA6.

Some information about the conformation of oxalamidines and AP can be derived from the absolute values of the scalar coupling constants $^1J_{^1H^{15}N}$. A large value indicates sp^2- and a small value sp^3- hybridization of the nitrogen atom.[49] The experimental values $-82.7, -93, -90,$[11] and -88[12] Hz for OA7, OA6, AP, and TPOA indicate that the compound with the most pronounced pyramidalization at the protonated nitrogen atoms is OA7. Hybridization of the nonprotonated nitrogen is expected to be close to sp^2. The proton transfer in OA7 should, therefore, be associated with a change of hybridization at the nitrogen atoms. This effect is less pronounced in the other oxalamidines.

The X-ray crystal structure of OA7 has recently been determined,[50] and the results of this study are shown in Figure 13. The mobile protons are localized on diagonal nitrogen atoms, and there is no sign of a solid-state tautomerism. The absence of the latter was confirmed by solid-state ^{15}N NMR experiments.[50] The mobile hydrogens are located in a plane containing the four nitrogen atoms and the two central carbon atoms. A substantially different pyramidalization of protonated and nonprotonated nitrogen atoms is not observed, a circumstance which may, however, be the result of solid-state interactions. The NH distance listed is probably too short as usual. Unfortunately, it was not possible to obtain crystals of OA5 and OA6 suitable for crystallographic studies.

(49) Binsch, G.; Lambert, J. B.; Roberts, B. W.; Roberts, J. D. *J. Am. Chem. Soc.* **1964**, *86*, 5564.

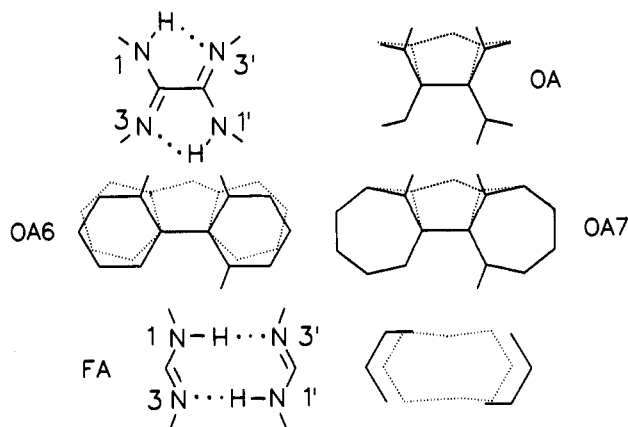(50) Scherer, G.; Lindner, H. J.; Limbach, H. H., unpublished.

Figure 14. Visualization of a structure-dependent reorganization of the molecular skeleton of the intramolecular tautomerism of oxalamidines and of the intermolecular tautomerism of formamidine dimers during the stepwise double proton transfer.

Structure-Dependent Skeleton Reorganization and Proton-Transfer Dynamics. Although the change of the hybridization at the nitrogen atoms during the proton transfer could play a role, it cannot explain the different behavior of the various oxalamidines. This also applies to the double–single bond shifts associated with the transfer. The strength of the intramolecular hydrogen bond seems to play an important role: the stronger the bond, the lower the activation energy of the transfer. Therefore, for a given compound the compression of the hydrogen bond in which the single proton transfer takes place will lower the barrier for the proton transfer. Since the hydrogen bond strength differs for the various oxalamidines, the compression will involve much less energy in TPOA than in OA6. Figure 14 depicts the expected associated changes of the molecular skeleton for different oxalamidines. It is assumed that in the intermediate only a proton is shifted but that the geometry of the other atoms is more or less equal to the atom positions in the initial state. Both states are represented by solid lines and differ only in the location of the proton transferred. The expected geometries of the transition states are represented by broken lines. In the case of the parent compound OA, which is also representative for the analog TPOA, one can expect that compression of the proton-transferring hydrogen bond does not alter the geometry of the other. By contrast, in OA6 the compression of one hydrogen bond is associated with either a strong deformation of the six-membered rings or an elongation of the non-proton-transferring hydrogen bond. Both phenomena may be responsible for the very high energy of activation of the tautomerism of OA6 which is absent in TPOA. The case of OA7 represents an intermediate. The seven-membered rings are expected to be less stiff than the six-membered rings of OA6, enabling easier compression of one hydrogen bond associated only with a small elongation of the other or with a ring deformation. One can thus explain the structural effects on the oxalamidine tautomerism in terms of substantial heavy atom reorganization of the molecular skeleton, leading to reduced primary kinetic isotope effects, as tunneling can only occur near the top of the barrier.

This interpretation is also consistent with the finding that secondary kinetic hydrogen/deuterium isotope effects S of the azophenine tautomerism[11] (Figure 1) and of the oxalamidine

tautomerism arising from the bound mobile proton are close to 1. This is because the vibrational frequencies of the bound mobile proton remain essentially constant in the transition state. The observation that S is slightly smaller than 1 is consistent with a small hydrogen bond elongation of the non-proton-transferring unit in the transition state, which slightly increases the vibrational frequencies of the bound mobile protons. This result is in contrast to the kinetic isotope effects observed in the intermolecular double proton transfer of diarylformamidines (FA, Figure 14), where replacement of the second H by D also leads to a substantial reduction of the rate constants.[10] When the FA data are interpreted in terms of a stepwise process, one has to assume that the bound mobile proton contributes a secondary H/D isotope effect S which is almost of the same size as the primary H/D isotope effect contributed by the proton in flight. This finding was also interpreted in terms of hydrogen bond compression in the transition state;[10] however, in contrast to the oxalamidine case, where compression of one hydrogen bond leads more or less to an elongation of the other bond, compression of one hydrogen bond of formamidine also leads to a compression of the other hydrogen bond, as illustrated in Figure 14. Therefore, the vibrational frequencies of the bound mobile proton are shifted to lower frequencies, leading to a secondary isotope effect whose size is so large that it can no longer be experimentally distinguished from a second primary isotope effect, typical for a concerted proton motion.

Conclusions

We have described the kinetic HH/HD/DD isotope and solvent effects on the tautomerism of the bicyclic oxalamidine derivative OA7, and both indicate a stepwise reaction pathway for this reaction. These results definitively establish the isotope method as a diagnostic tool for the distinction of stepwise and concerted degenerate double proton-transfer reactions. This tool is especially useful when kinetic solvent effects are absent and when temperature-dependent experiments cannot be performed. The relatively small kinetic hydrogen/deuterium isotope effects of the tautomerism of OA7 can be interpreted in terms of a substantial heavy atom reorganization preceding proton tunneling near the top of the barrier. This reorganization consists of hydrogen bond compression, ring deformation, and solvent reorientation in the transition state and can also explain the observed dependence of the oxalamidine tautomerism on the chemical structure.

Supplementary Material Available: Tables 3–5, containing all numerical data obtained by data analysis of the NMR experiments described in this study (4 pages). This material is contained in many libraries on microfiche, immediately follows this article in the microfilm version of the journal, and can be ordered from the ACS; see any current masthead page for ordering information.